Broadly-tunable (993-1110 nm) Yb:YLF laser

Preprint · February 2022

CITATIONS
0

READS
28

6 authors, including:

Umit Demirbas
Antalya Bilim University
157 PUBLICATIONS **1,440** CITATIONS
SEE PROFILE

Jelto Thesinga
Deutsches Elektronen-Synchrotron
36 PUBLICATIONS **116** CITATIONS
SEE PROFILE

Simon Reuter
Deutsches Elektronen-Synchrotron
15 PUBLICATIONS **14** CITATIONS
SEE PROFILE

Broadly-tunable (993-1110 nm) Yb:YLF laser

UMIT DEMIRBAS,[1,2,*] JELTO THESINGA,[1] MARTIN KELLERT,[1] SIMON REUTER,[1] MIKHAIL PERGAMENT[1] AND FRANZ X. KÄRTNER[1,3,4]

[1]*Center for Free-Electron Laser Science CFEL, Deutsches Elektronen-Synchrotron DESY, Notkestr. 85, 22607 Hamburg, Germany*
[2]*Laser Technology Laboratory, Department of Electrical and Electronics Engineering, Antalya Bilim University, 07190 Dosemealti, Antalya, Turkey*
[3]*Physics Department, University of Hamburg, Luruper Chaussee 149, 22761 Hamburg, Germany*
[4]*The Hamburg Centre for Ultrafast Imaging, Luruper Chaussee 149, 22761 Hamburg, Germany*
**uemit.demirbas@cfel.de*

Received XX Month XXXX; revised XX Month, XXXX; accepted XX Month XXXX; posted XX Month XXXX (Doc. ID XXXXX); published XX Month XXXX

We have investigated room-temperature continuous-wave (cw) lasing performance of Yb:YLF oscillators in detail using rod-type crystals with low Yb-doping (2%). The laser is pumped by a low-cost, high brightness 10-W, 960 nm single-emitter multimode diode. Laser performance is acquired in both E//a and E//c axes, using twelve different output couplers with transmission ranging from 0.015% to 70%. We have estimated the passive loss of the Yb:YLF crystal as 0.06% per cm, corresponding to an impressive crystal figure of merit above 4000. The low-doping level not only reduces the system losses, but also minimizes the thermal load as the lowly doped crystals enable distribution of heat load in a greater volume. Using the advantages of lower-loss and improved thermal behavior, we have achieved cw output power above 4 W, cw slope efficiencies up to 78% and a record cw tuning range covering the 993-1110 nm region (117 nm). The output power performance achieved in this initial work is limited by the available pump power, and future Yb:YLF systems has the potential to produce output power levels above 10 W level.

http://dx.doi.org/10.1364/OL.99.099999

1. Introduction

Yb:YLF have been attracting the attention of researchers working in laser-cooling (optical refrigeration) [1–7] and laser/amplifier development fields [8–17] over the last 2 decades. One important reason for this interest is the capability to grow high-quality Yb:YLF crystals with minimal passive losses [6]. Especially, for the optical refrigeration community, to achieve optical cooling, extremely high purity samples with high external quantum efficiency are necessary [18]. Using Yb:YLF samples with background absorption as low as $2x10^{-4}$ cm^{-1}, laser cooling of the samples down to 114 K has been demonstrated [18]. High-quality laser crystals also enable efficient lasing performance with minimal intracavity losses, that is quite important for several applications, including low timing-jitter noise laser oscillator development [19–21].

Room-temperature (RT) lasing of Yb:YLF has been investigated in several different geometries (rod, thin-disk, and waveguide). In their initial lasing work, using a 0.3 mm long 40.5% doped crystal, Kawanaka et al. achieved 50 mW of continuous-wave (cw) output power around 1040 nm at an absorbed pump power of 400 mW using a 1.5% output coupler [8]. After this initial demonstration, with the development of higher brightens diodes and higher quality crystals and cavity optics, the performance of Yb:YLF lasers improved significantly and cw output power levels as high as 3.03 W [22], 2.76 W [23] and 5.87 W [24,25] were achieved at room temperature from rod, waveguide and thin-disk geometries, respectively. A slope efficiency as high as 76% was demonstrated under Ti:Sapphire pumping [23]. Continuous-wave tuning ranges covering the 993-1076 nm region was also achieved [26]. Moreover, via cooling the crystal to cryogenic temperatures [9,15,27–29] cw output power above 500 W [16], and slope efficiencies as high as 82% [30] were demonstrated at the expense of reduced gain bandwidth (tuning range: 995-1020.5 nm [31]).

In this work, we have investigated cw lasing performance of 2%-Yb-doped YLF crystals in great detail at room temperature. We have seen that, at this low doping level, the crystals have very low passive losses of 0.06% per cm enabling efficient laser operation. Upon pumping the laser with a high brightness 10-W single-emitter multimode diode at 960 nm, we have achieved cw power up to 4 W, a slope efficiency of 78% and a record cw tuning range covering the 994-1110 nm region. This tuning performance is among the broadest tuning ranges yet reported from Yb-based solid state lasers [32], and show the potential of Yb:YLF crystals for the

development of efficient short pulse (sub-20-fs [33]) oscillators with ultralow timing jitter [34].

The paper is organized as follows: In Section 2, we present the setup we have used in lasing experiments. In Section 3, we provide details of cw laser efficiency and laser crystal loss estimate. Later, in Section 4 we report our cw tuning results, and discuss the tuning performance by comparing it with the measured gain spectra. Finally, in section 5, we conclude with a brief summary and provide an outlook for future progress.

2. Experimental setup

Figure 1 shows a schematic of the Yb:YLF laser that is used in continuous-wave laser experiments. A single-emitter multimode diode (MMD) providing up to 10 W of pump power at 960 nm is used for pumping. The MMD has an emitter size of 1×100 µm (sagittal/fast × tangential/slow axes), and provides a quite asymmetric rectangular shaped multi-transverse mode beam. The MMD output beam is first collimated with a 4.5 mm focal length aspheric lens (f_1), then to minimize the diode beams astigmatism a cylindrical lens with a focal length of 50 mm (f_z, acting on the fast axis) is employed. An achromatic doublet with a focal length of 80 mm (f_2) is utilized to focus the pump beam to a waist of around 25 µm x 100 µm inside the crystal. Brewster-Brewster cut, 2% Yb-doped 10 mm and 15 mm long YLF crystals with a width of 5-mm and thickness of 2 mm are used for the lasing experiments in E//c and E//a axes, respectively (Fig. 2). The estimated small-signal absorption of crystals for TM polarized light at 960 nm is 81% and 94% for the 15 mm (E//a) long and 10 mm (E//c) long Yb:YLF crystals. To improve the absorption of the E//a cut crystal, pump polarization is rotated using a half-wave plate, to achieve a small signal absorption of around 98.5% for the TE polarized light (at the expense of 10% reflection loss from the crystals Brewster surface). The crystals are mounted with indium foil in a copper holder under water cooling at 15 °C.

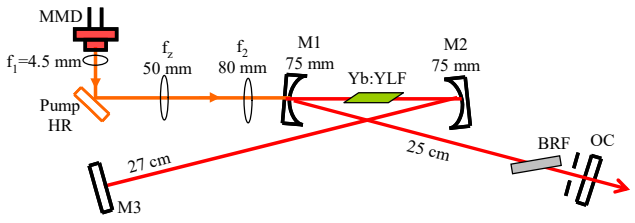

Fig. 1. Experimental setup of the diode-pumped Yb:YLF laser used in cw laser experiments. BRF: Birefringent filter, OC: Output coupler, MMD: 10-W, 960 nm, single-emitter multimode laser pump diode.

A standard X-type resonator is used in cw laser experiments. The laser cavity consisted of two curved high reflector mirrors, each with a radius of curvature of 75 mm (M1 and M2), a flat end high reflector (M3), and a flat OC. The arm lengths for the high-reflector and OC end are 27 cm and 25 cm respectively, resulting in a beam waist of ~30 µm x 40 µm inside the crystal. The pump mirrors (M1-M2) are anti-reflection coated the 800-970 nm range (R<2%). All the cavity high reflectors (M1-M3) have reflective coatings covering the 1010-1200 nm spectral region with a reflectivity above 99.9% specified at 0° incidence (Layertec mirror: 102924). The mirrors M1-M2 are used at an incidence angle of around 10-15°, which slightly blue shifted the reflectivity band specified above. Twelve different output couplers with transmission ranging from 0.015% to 70% are used in the experiments to carefully scan the operation range of the lasers. An adjustable width mechanical slit is inserted near the output coupler to control the transverse output mode of the laser in the tangential axis.

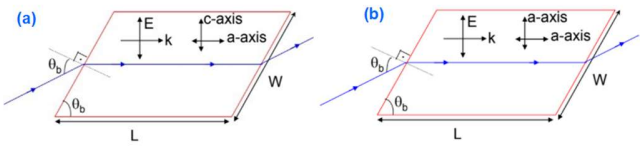

Fig. 2. Top view of Brewster-Brewster cut Yb:YLF crystals optimized for lasing in (a) E//c and (b) E//a axes, respectively. Path of a TM polarized light is shown in blue. E: electric field vector, k: beam propagation direction, θ_b: Brewster's angle, L: Length of the laser crystal, W: Width of the crystal, H: height/thickness of the crystal (not visible in the picture).

A 2-mm thick off-surface optical axis crystal quartz birefringent filter (BRF) with a diving angle of 25° is inserted at Brewster's angle near the output coupler for smooth tuning of laser wavelength [35]. The TE-polarized intracavity beam have Fresnel reflection losses from the laser crystal and the BRF plate surfaces, which provides a modulation depth of around 40% in one round trip. While operating around 1000 nm, the BRF has a calculated free-spectral range of around 350 nm, a filter full width half-maximum (FWHM) of around 40 nm, and a tuning rate of around 45 nm per degree (calculated parameters are for the 2nd order of the BRF, around a rotation angle of 35°).

3. Continuous-wave lasing results

Figure 3 shows the measured efficiency of Yb:YLF laser using output couplers with transmission ranging from 0.015% to 60% for both (a) E//a and (b) E//c axes. Using E//a axis, the optimum cw performance is obtained with a 1% transmitting output coupler. At this output coupling, we have measured a lasing threshold of around 0.5 W, and the laser produce a cw output power of 3.1 W around 1040 nm at an absorbed pump power of 8 W (absorption: 94.8%). The slope efficiency curve is nonlinear due to the 3-level structure of the gain medium [36]. The laser reaches a slope efficiency of 54% (with respect to absorbed pump power) at high pump intensities.

For the E//c axis, using the same 1% output coupler, we have measured a lasing threshold of only around 0.2 W due to higher gain in the E//c axis [37]. At 1% coupling, the E//c axis lasing results in an output power of 3.67 W around 1050 nm at an absorbed pump power of 8.5 W (absorption:91%). With the E//c axis, a better cw performance is achieved using the 5% transmitting output coupler. While employing the 5% OC, we have measured a cw lasing threshold of around 0.75 W, and obtained a cw power of 4 W at an absorbed pump power of 8 W. The slope efficiency curve is again quite nonlinear: the slope efficiency starts at 30% and increases up to 78% at high pump power levels. This we believe is one of the highest slope efficiencies obtained from Yb:YLF lasers to date [23,30].

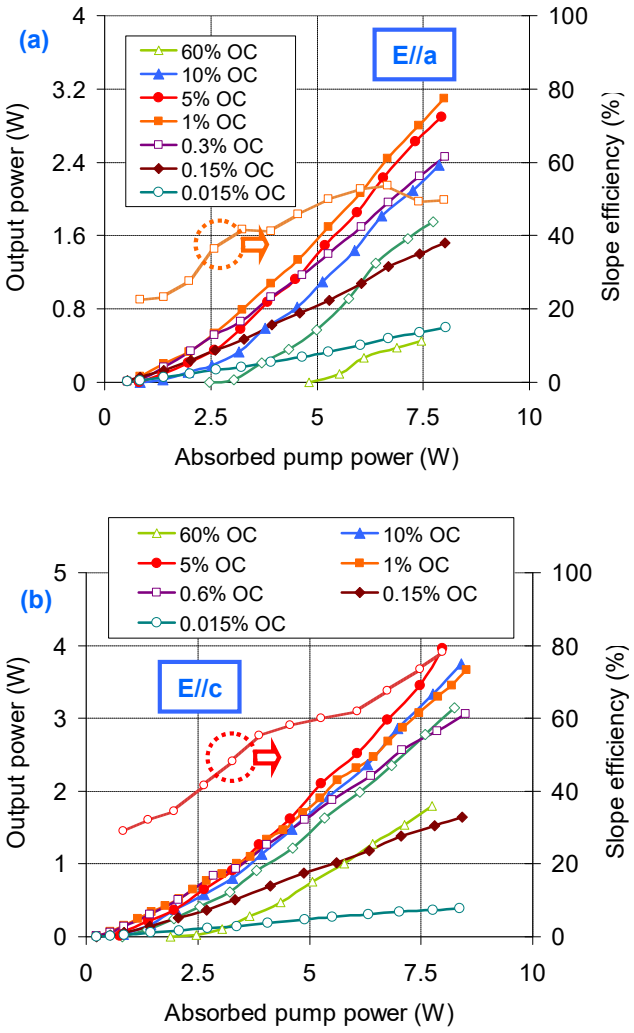

Fig. 3. Measured cw laser performance of the room-temperature Yb:YLF laser using output couplers in the 0.015% to 60% range for (a) E//a and (b) E//c axis; respectively. Variation of slope efficiency with absorbed pump power level is also shown for the best performing output couplers: 1% OC for E//a and 5% OC for E//c axes, respectively.

We believe that the increase of slope efficiency with pump power is partly due to the 3-level laser structure, and partly due to changes in the laser transverse mode. As we will discuss later (using Fig. 6), as the pump power is increased, the laser output becomes multimode. This improves the mode-matching between the pump and laser modes and hence also the slope efficiency at high pump power levels. As another interesting observation, note that for large output coupling (such as the 60% shown in Fig. 3), we have observed a decrease in slope efficiency. This phenomenon is also observed in earlier work to some extend [13,16,31], and might be due to effects such as Auger upconversion, and pump excited stated absorption [36]. These process is weak in Yb-systems due to the simple energy level diagram. On the other hand, the emission observed at visible wavelengths in Yb:YLF clearly shows the presence of such mechanisms [38], and change of rate of these process with output coupling might be affecting the laser performance at large output coupling values. As a side note, in our experiments, we have observed that the greenish visible emission of Yb:YLF under tight pumping shifts to blue region of spectrum while using low output coupling values, that shows the role of inversion and intracavity power levels in these dynamics. Future work is required for better understanding of this phenomena.

In Figure 4, we plot the variation of cw output power performance and free-running laser wavelength with output coupling for both axes. Note that, some of the results that are shown in Fig. 4 is not included in Fig. 3, to not over-crowd the efficiency data (out of the twelve output couplers used, we have selected 8). As we discussed earlier, the optimum output coupling is around 5% for the E//c axis and around 1% for the lower gain E//a axis. The variation of performance with output coupling is rather smooth, and we could achieve similar cw performance for output coupling values in the 0.5-5% range for E//a axis, and 0.5-30 % range for E//c axis. As an interesting observation, while employing E//c axis, rather efficient laser operation could be achieved even at a coupling of 70%, which shows the high gain nature of the Yb:YLF material.

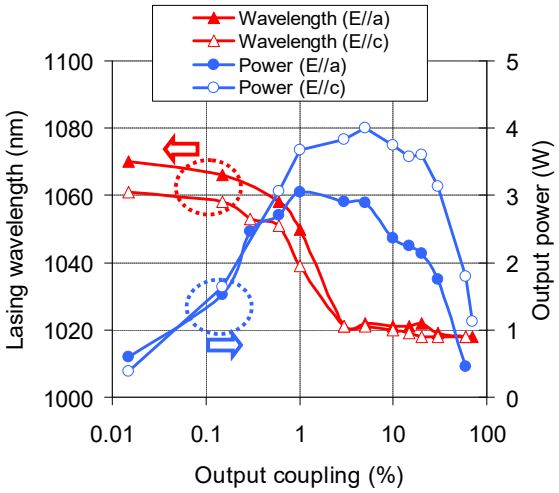

Fig. 4. Measured variation of free running laser wavelength and maximum attainable cw laser power with output coupling transmission. The data is taken while pumping the room-temperature Yb:YLF laser with an incident pump power of 9.87 W.

Note that, obtainable output power levels are higher in E//c axis for almost all output coupling values due to lower lasing thresholds and higher slope efficiencies acquired in this axis. The lower lasing threshold of E//c axis is clearly mostly due to the higher gain in this axis as already mentioned. On the other hand, the superior performance in terms of laser slope efficiency might be due to the better mode-matching that could be acquired in the shorter crystal length employed for E//c axis lasing (a 10 mm long crystal is used in E//c axis, compared to the 15 mm crystal used in E//a axis).

In terms of the free-running laser wavelength, both crystal axes behave rather similar: as the output coupling is increases the free running laser wavelength shifts from around 1060-1070 nm to around 1020 nm region (Fig. 4). This observation is in relatively

good agreement with earlier reports in literature [13,26], and will be discussed in more detail in the next section. As a side note, we see that, at low output coupling values (below 3%), the free running laser wavelengths are slightly longer in E//a axis compared to the E//c axis (e.g. 1070 nm in E//a and 1061 nm in E//c using the 0.015% transmitting output coupler). This might be due to the lower gain in E//a axis: the self-absorption losses push the laser wavelength more towards the longer wavelength side of the emission spectrum.

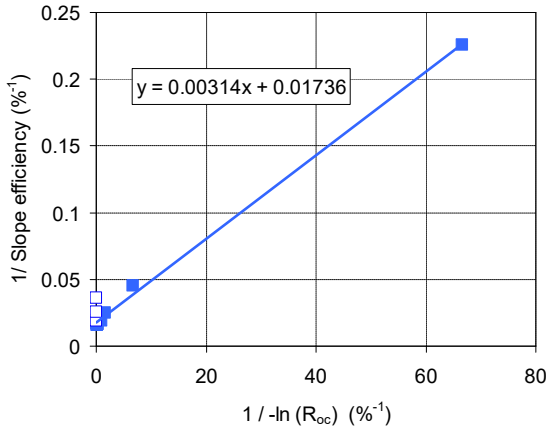

Fig. 5. Measured variation of the inverse of the slope efficiency with the inverse of the output coupling percentage for the Yb:YLF laser employing the E//c axis. Using Caird analysis, making a best-fit to the measured data (blue solid curve), we have estimated the round-trip passive cavity loss to be 0.18 ±0.05%. For the slope efficiency values, a linear fit is made to the laser efficiency data, and in this fit only data points above 5 W absorbed pump power level is taken. Slope efficiency data for the 60% and 70% output couplers are considered outliers (shown with open markers in the graph), and is not included in the analysis. R_{oc}: Reflectivity of the output coupler.

We have also utilized the measured variation of the laser slope efficiency with output coupler transmission to estimate the level of passive cavity losses (Caird analysis [39]), and find that the round-trip passive loss of the system is around 0.18 ±0.05% (Fig. 5). Assuming around 0.06% of this loss comes from cavity optics (2 bounces on M1-M2, and one bounce on M3 and OC: 6 overall bounces), for the 10 mm 2% Yb-doped crystal, we estimate a passive loss of around 0.06±0.02% per cm (effective loss coefficient: 0.0006 cm^{-1}). Note that this loss level is lower than, the passive losses that are estimated for Cr:LiCAF/Cr:LiSAF crystals (0.1-0.2 % per cm), and is similar to the values one can get in good quality Alexandrite samples (0.06 % per cm [40]). On the other hand, for a more practical/useful comparison between different laser gain media, it is better to compare the figure of merit (FOM) parameter of different crystals. FOM of a crystal is defined as the ratio of absorption coefficient at the pump wavelength to the effective passive loss coefficient at lasing wavelength (this ignores self-absorption losses). The 2% Yb-doped YLF crystal we have employed in this study has an absorption coefficient of around 2.8 cm^{-1} at 960 nm for E//c axis at room temperature [37]. Overall, then the FOM of the Yb:YLF crystal is above 4000 (2.8/0.006 ≅4667). For comparison, in a carefully performed earlier study, Pirzio et al. estimated a round-trip passive loss of around 0.34% for a Yb:YLF laser employing a 2.1 mm thick 10 % Yb-doped YLF crystal [13]. Under similar assumptions, we estimate a passive loss of around 0.7% per cm and a FOM of around 2000 for the 10% Yb-doped YLF sample used in [13]. We believe the higher FOM of the crystals used in this study might be due to the lower Yb-doping employed in our case.

It is educational to compare the estimated FOM of Yb:YLF with other common laser materials. For example, the figure of merit of commonly employed Ti:Sapphire crystals is just around 250 [41], and only carefully hand selected samples could reach FOM values up to 1000 [42]. The FOM of carefully-grown Cr:LiCAF crystals are around 2000, and for Cr:LiSAF and Alexandrite the FOM could reach 3000 [43]. Having such a low loss crystal with extremely high FOM, enables construction of high-Q-cavities, which has benefits in optimizing intracavity experiments such as intracavity second harmonic generation. Such high-Q systems could also be used in designing femtosecond oscillators with pulse train timing jitter noise levels below 100 attoseconds [20]. Of course, as discussed earlier, Yb:YLF crystals with high FOM also provide advantages to the laser-cooling community [6].

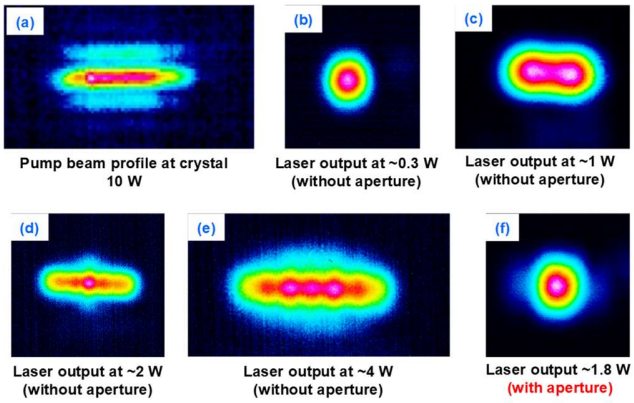

Fig. 6. (a) Measured pump beam profile at the position of the crystal at the maximum pump power level (10 W). (b-e) Laser output beam profile just after the OC at several different output power levels. Without the intracavity slit, the laser output mode starts to acquire higher transverse mode orders at increasing power levels. (f) Adjusting the width of the intracavity slit in the tangential plane enables TEM_{00} laser output, at the expense of reduced output power: the laser power decreases from 4 W to 1.8W at 10 W incident pup power.

Due to the multimode pump beam, the output of the Yb:YLF laser is also multi transverse mode, as we have also observed in earlier multimode diode pumped systems such as Cr:LiCAF and Cr:LiSAF [43]. Figure 6 (a) shows the beam profile of the pump diode at its maximum power setting (10 W), which is quite asymmetric mainly due to the asymmetry of the diode emitter size. The Yb:YLF laser output beam profile at different output power levels is shown in Fig. 6 (b-e). As the pump power is increased, the pump beam itself contains higher transverse order modes, and in response the Yb:YLF laser, which starts with a TEM00 beam at low output power levels (0.3 W), becomes highly multi-transverse

mode at increasing pump power levels. The observed variation of the output beam profile of the Yb:YLF laser enables efficient mode-matching between the pump and laser modes, and as discussed earlier, this process is partially responsible for the larger laser slope efficiencies observed at higher pump power levels. In our experiments, we have tried implementing an intracavity slit near the output coupler mirror, and by adjusting its width in the tangential plane, it was possible to push the Yb:YLF laser to produce a symmetric beam with a TEM_{00} profile. However, this comes at the expense of reduced mode-matching, and hence reduced output power levels. In this mode (Fig. 6 (f)), the Yb:YLF laser only produced 1.8 W of output power at the 10W incident pump power. For comparison, we have recently investigated the laser performance of a highly Yb-doped (25%) 1.5 mm long crystal in the same laser cavity. The laser performance was inferior in this highly doped sample (around 3 W compared to 4 W in this work) [22]. However, the short crystal enabled better mode matching between the pump and laser modes compared to the 10-15 mm long crystals used in this study, and the laser output beam quality was superior. Hence, depending on the intended application, one needs to carefully optimize the doping and length of the crystals for control of the laser behavior.

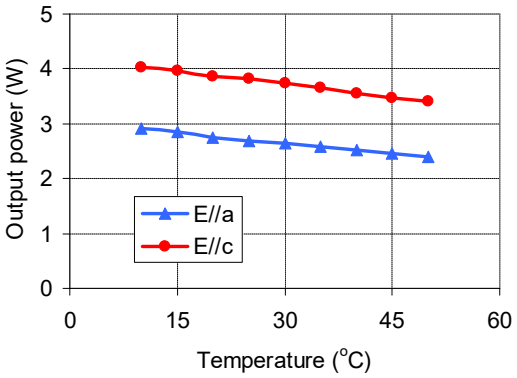

Fig. 7. Measured variation of Yb:YLF laser output power with laser crystal holder temperature for E//a and E//c axes. The data is taken at an incident pump power of 9.87 W using a 5% transmitting output coupler.

In closing this section, we would like to mention that, in our cw laser experiments with Yb:YLF, we have not yet observed limitations due to thermal effects, even at the maximum pump power level (10 W) that is available from the system. This is partly due to the lowly Yb-doped YLF samples used in this study, which enables a good distribution of thermal load in the relatively long crystals employed in this work. Especially, we have not noticed presence of thermal lensing, which is a known advantage of YLF host compared to other hosts like YAG [44–51]. The experimental data in Figs. 3 and 4 is taken at a crystal holder temperature of 15 °C. However, we have also investigated variation of laser output power with crystal holder temperature, in the temperature range of 10-50 °C. As we can see from Fig. 6, as the temperature of the Yb:YLF crystal holder is increased, the obtainable laser output power levels slowly decrease with temperature for lasing in both axes. This decrease of output power with temperature is mainly due to the decreasing emission cross section value (as the intrinsic lifetime of the Yb:YLF material is constant over a wide temperature range) [37,38]. Based on our observations, we believe that, in future studies, using higher power pump diodes, the output power levels obtainable from room-temperature Yb:YLF lasers could be scaled to above 10 W even in simple rod geometry, and to multi-10s of W level in thin-disk geometry.

4. Continuous-wave tuning results

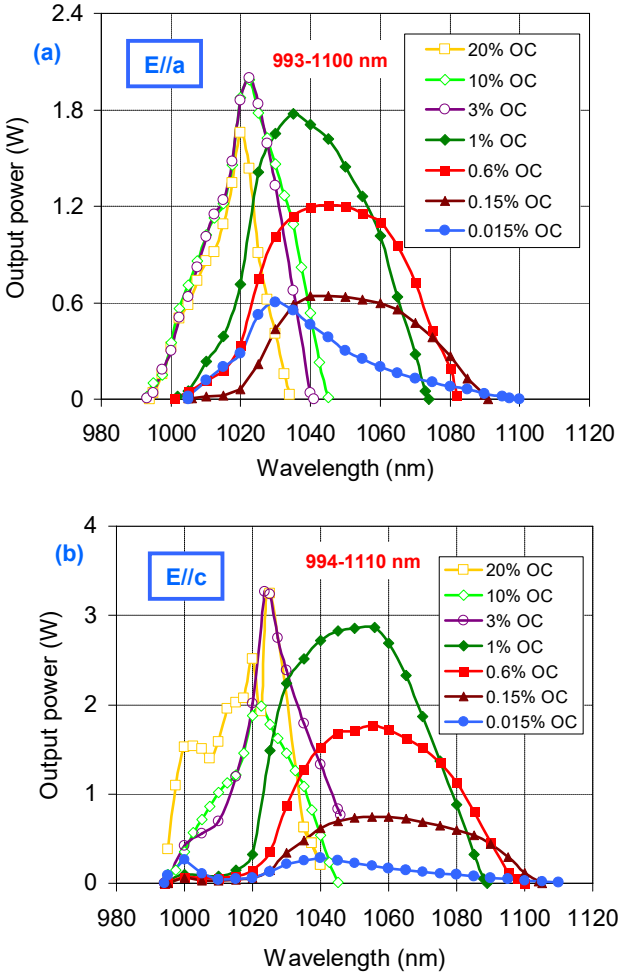

Fig. 8. Measured tuning behavior of the cw Yb:YLF laser using output couplers in the 0.015% to 20% range for (a) E//a and (b) E//c axis; respectively. The data is taken at an incident pump power of 9.87 W. The overall tuning range covers the 9913-1110 nm region (117 nm).

The detailed cw laser efficiency measurements we have made showed that the lowly Yb-doped YLF samples employed in this study has very low passive losses. Motivated with this, we have explored the cw tuning capabilities of the laser in both axes using an intracavity birefringent filter. Tuning of the laser wavelength is facilitated simply by rotation of the birefringent plate about an axis normal to the surface, and the process do not require laser realignment. Moreover, since the BRF is inserted at Brewster's

angle inside the laser cavity, it does not require anti-reflective coatings, and its passive losses is rather low.

Figure 8 shows the measured cw tuning behavior of the room-temperature Yb:YLF laser for both E//a and E//c axes, at an incident pump power of 9.87 W. Tuning data is taken with several different output couplers with transmissions in the 0.015-20%, range. With the E//a axis, using a 1% output coupler, the Yb:YLF laser is tunable in the 1000-1075 nm range, and cw power levels up to 1.8 W could be obtained. For comparison, using the same OC, we could achieve a tuning range from 995 nm to 1089 nm, and a cw power up to 2.9 W with the E//c axis. Clearly, due to its higher gain, the E//c axis provides a broader tuning range when one employs same output coupling. For pushing the long wavelength operation limit, we have used a 0.015% transmitting output coupler, where cw tunings ranges of 1005-1100 nm and 994-1110 nm are demonstrated for E//a and E//c axis, respectively. For the E//a axis, the short wavelength tuning limit could be reduced down to 993 nm using output couplers with transmissions values above 3%. Figure 9 shows sample optical spectra taken during the tuning experiments. To our knowledge, this study reports the first demonstration of lasing of Yb:YLF above 1075 nm [20]. This we believe is due to the low-loss cavities employed in this study.

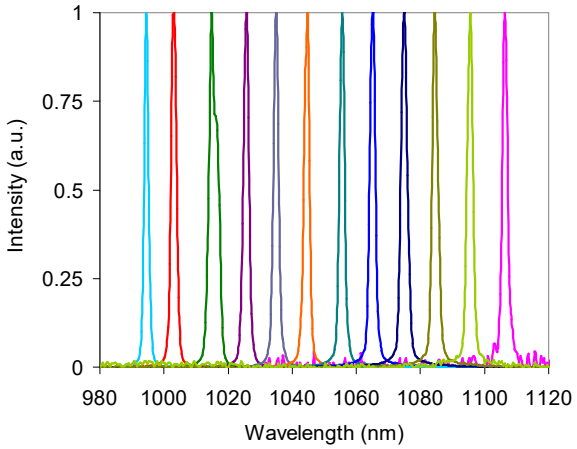

Fig. 9. Sample optical spectra demonstrating cw tunability of the Yb:YLF laser in the 993-1110 nm region.

Note that for the E//c axis, while employing output couplers with transmission above 3%, the tuning modulation depth of the BRF (40%) was not high enough to enable smooth tuning: as one can see form Fig. 8 (b) the tuning curves are not always complete. As an example, suing the 3% output coupler, while trying to tune the laser above 1045 nm, we have observed wavelength jumps to the gain peak (~1020 nm). Basically, the laser preferred to operate at 1020 nm with TE polarization instead of operating at 1050 nm with TM polarization. This shows that, the 40% modulation depth we have in the system is not sufficient to suppress this jump due to large differences in gain. Hence, in future studies, design of higher modulation depth systems could smoothen the tuning of the E//c axis laser at high output coupling values.

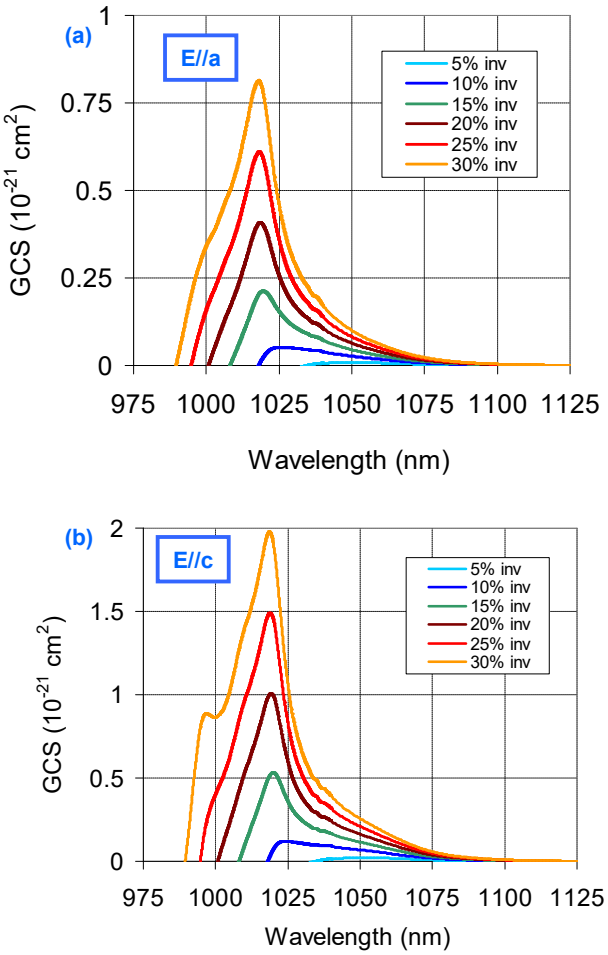

Fig. 10. Calculated room-temperature gain cross section (GCS) spectra for Yb:YLF at inversion levels between 5 and 30% for (a) E//a and (b) E//c axes, respectively.

As one can see from Fig. 8, the tuning behavior is quite diverse at different output coupling values. First of all, as the output coupling is increased, the wavelength at which the maximum output power could be attained, start to shift to shorter wavelengths. This observation is in good agreement with the variation of free running laser wavelength with coupling, as it is outlined earlier in Fig. 4. Moreover, at increased output coupling, the obtainable tuning range gets narrower. This behavior is due to the three-level laser structure of Yb:YLF gain medium, and could be understood by investigating the room-temperature gain spectrum. Fig. 10 shows the calculated variation of gain cross section (GCS) with wavelength for both axes of Yb:YLF for inversion levels between 5% and 30%. The gain cross section spectra ($\sigma_g(\lambda)$) are estimated using the measured emission spectra [37] via the following formula:

$$\sigma_g(\lambda) = \beta\sigma_e(\lambda) - (1-\beta)\sigma_a(\lambda) \qquad [1]$$

where λ is the wavelength, σ_e (σ_a) is the emission (absorption) cross section, and β is the fractional population inversion level. The estimated GCS curves are in relatively good agreement with the previously reported curves in literature [12,26]. We can see from Fig. 10, as the inversion of the crystal increases, the peak of the gain spectra shifts to shorter wavelengths due to reduced self-absorption losses.

Note that, at increasing output coupling, one increases the overall loss of the cavity, and hence to balance the increased loss, the crystal possesses a higher level of inversion at high output coupling values. As a result, at increased output coupling, the losses and inversion of the crystal increases, and one expects a blue shift of laser wavelengths. Hence, this first observation explains the wavelength shifts we have observed in Fig. 4 and Fig. 8. As a second observation, we see that, at high inversion levels, gain curves get sharper and the FWHM of the gain curve decreases. This second observation explains the narrower tuning range behavior we have observed at higher output coupling.

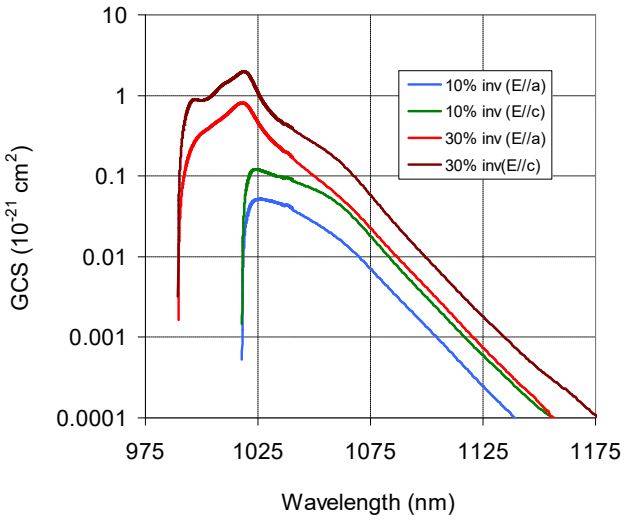

Fig. 11. Calculated room-temperature gain cross section spectra for Yb:YLF at inversion levels of 10% and 30% for E//a and E//c axis.

As another observation, we see from Fig. 10 that, the gain at the longer wavelength edge of Yb:YLF is rather small. As a result, to achieve lasing in this region, we had to use an output coupler with minimal loss (0.015%) to acquire lasing in this region. To look at this in detail, Fig. 11 shows the GCS curve for E//c and E//a axis together in the same graph, at selected inversion levels of 10 and 30%. From Fig, 11, we clearly see that, the gain of Yb:YLF around 1100 nm is more than 2 orders of magnitude lower compared to the gain around 1020 nm for both polarizations. This explains the tuning behavior we have observed in the long wavelength side (Fig. 8): the long wavelength tuning range could be improved by employing output couplers with lower transmission. As an example, for the E//c axis, we have obtained cw tuning limits of 1074 nm, 1082 nm, 1090 nm and 1110 nm at output coupling values of 1%, 0.6%, 0.15% and 0.015%. We also see form Fig. 11 that, on the long wavelength side, the E//c axis gain spectra extends to longer wavelengths compared to E//a axis (for a fixed inversion/pump level), and this explains the slightly broader tuning we have achieved while employing the E//c axis (1110 nm in E//c axis versus 1010 nm in E//a axis). As another observation, note from Fig. 11 that, on the short wavelength side, the GCS spectra drops sharply around 990 nm for both for E//a and E//c axis due to increased role of self-absorption losses, and this matches well with the short-wavelength tuning limit that is observed int his study (993 nm).

4. Conclusions

Yb-doping, crystal axis, crystal geometry	Max cw slope efficiency [%]	Max cw output power [W]	Tuning range, or operating wavelength (nm)	Ref. and year
15, //c, rod	25	0.25	1017-1052	[52], 00
40.5, //c, rod	50	0.05	1025-1050	[7], 01
30, //c, rod	31	1.15	1022-1074	[10], 07
	63§	4§		
5%, //a, rod	29	0.27	1009-1061	[53], 08
5%, //c, rod	33	0.36	1011-1069	
10%, //c, rod	-	-	1013-1066§	[54], 09
30%, //c, rod	~35	~0.7	997-1075§	[55], 09 [56],10
30%, //a, rod	56§	3.69§	993-1065§	[26], 10
30%, //c, rod	59§	4.5§	995-1076§	
30%, //c, TD	42	5.87	1047	[24,25], 11
~3.3%,//c, waveguide	41	0.292	1019.5	[23], 13
	76	0.540	994.4	
	43	2.76	1020	
10%, //a, rod	58.6	0.126	1040	[13], 16
10%, //c, rod	58.5	0.129	1030	
25%, E//c, rod	50	3.03	997-1075	[22], 22
2%, //a, rod	54	3.1	994-1110	*, 22
2%, //c, rod	78	4	993-1100	

Table 1: A summary of room-temperature continuous-wave lasing results obtained with Yb:YLF material. § Results obtained in quasi-cw regime. *Indicates results obtained in this work.

We would like to finalize our paper with Table 1, which provides a summary of the cw room-temperature lasing results obtained with Yb:YLF lasers to date. We see from the table that, this study reports room-temperature lasing results using crystals with a lower amount of Yb-doping compared to earlier work. Most probably, as a result of this low-doping level, the crystals used in this study had very low passive losses. Usage of low-loss crystals with rather long length also enabled distribution of the thermal load in a greater volume and reduces thermal effects. As a result, in this study we have generated cw power up to 4 W from the system, which is the highest reported true cw power to date in rod geometry at room-temperature. The power level is limited by the available pump power, and we believe future diode-pumped room-temperature Yb:YLF systems could scale the output power levels above 10 W even in simple rod geometry. Despite the asymmetric pump diode we have employed in this work, we have observed slope efficiencies up to 78%, which is similar to what is achieved with Ti:Sapphire pumping (76% in [23]). By taking advantage of the lower crystal

losses, we have also extended the cw tuning range of Yb:YLF lasers considerably, and achieved smooth cw tuning in the 993-1110 nm range (117 nm, 35 nm extension on the long wavelength side, compared to earlier tuning results). For comparison cw tuning ranges of 987-1134.5 nm (147.5 nm, Yb:Lu_2O_3 [32]), 999-1089 nm (Yb:CALGO, 90 nm [57]), 992-1095 nm (103 nm, Yb:LuAG [58,59]), 992.5-1111 nm (118.5 nm, Yb:YAG [60]), 1017-1086 nm (69 nm, Yb.BOYS [61]), 1018-1072 nm (54 nm, Yb:CaF_2 [62]), ~1005-1078 (73nm, Yb:SrF_2 [63]) and 1018-1088 nm (70 nm, Yb:SYS [64]) are reported from other Yb-based systems. Comparing with these results, we see that, the tuning range we have acquired with Yb:YLF (993-1110 nm, 117 nm) is among the broadest tuning ranges yet reported from Yb-based solid state lasers, which shows its potential as a solid-state ultrafast laser and amplifier.

Funding
Seventh Framework Programme (FP7) FP7/2007- 2013
European Research Council (ERC) Synergy Grant (609920).

Disclosures
The authors declare no conflicts of interest.

Data Availability

Data underlying the results presented in this paper are not publicly available at this time but may be obtained from the authors upon reasonable request.

REFERENCES

1. D. V Seletskiy, S. D. Melgaard, S. Bigotta, A. Di Lieto, M. Tonelli, and M. Sheik-Bahae, "Laser cooling of solids to cryogenic temperatures," Nat. Photonics **4**, 161–164 (2010).
2. D. V Seletskiy, S. D. Melgaard, R. I. Epstein, A. Di Lieto, M. Tonelli, and M. Sheik-Bahae, "Local laser cooling of Yb:YLF to 110 K," Opt. Express **19**, 18229–18236 (2011).
3. A. Di Lieto, A. Sottile, A. Volpi, Z. H. Zhang, D. V Seletskiy, and M. Tonelli, "Influence of other rare earth ions on the optical refrigeration efficiency in Yb:YLF crystals," Opt. Express **22**, 28572–28583 (2014).
4. S. Püschel, S. Kalusniak, C. Kränkel, and H. Tanaka, "Temperature-dependent radiative lifetime of Yb:YLF: refined cross sections and potential for laser cooling," Opt. Express **29**, 11106 (2021).
5. G. Cittadino, A. Volpi, A. Di Lieto, and M. Tonelli, "Co-doping of LiYF4 crystal: a virtuous effect of cooling efficiency," J. Phys. D-Applied Phys. **51**, (2018).
6. G. Brasse, P. Loiko, C. Grygiel, A. Benayad, F. Lemarie, V. Zakharov, A. Veniaminov, J. L. Doualan, A. Braud, and P. Camy, "Liquid Phase Epitaxy growth, structure and spectroscopy of highly-doped 20 at.% Yb3+:LiYF4 thin films," J. Lumin. **236**, 118071 (2021).
7. A. Pant, X. J. Xia, E. J. Davis, and P. J. Pauzauskie, "Solid-state laser refrigeration of a composite semiconductor Yb:YLiF4 optomechanical resonator," Nat. Commun. **11**, (2020).
8. J. Kawanaka, H. Nishioka, N. Inoue, and K. Ueda, "Tunable continuous-wave Yb : YLF laser operation with a diode-pumped chirped-pulse amplification system," Appl. Opt. **40**, 3542–3546 (2001).
9. J. Kawanaka, K. Yamakawa, H. Nishioka, and K. Ueda, "Improved high-field laser characteristics of a diode-pumped Yb : LiYF4 crystal at low temperature," Opt. Express **10**, 455–460 (2002).
10. J. Kawanaka, K. Yamakawa, H. Nishioka, and K. Ueda, "30-mJ, diode-pumped, chirped-pulse Yb : YLF regenerative amplifier," Opt. Lett. **28**, 2121–2123 (2003).
11. M. Vannini, G. Toci, D. Alderighi, D. Parisi, F. Cornacchia, and M. Tonelli, "High efficiency room temperature laser emission in heavily doped Yb : YLF," Opt. Express **15**, 7994–8002 (2007).
12. N. Coluccelli, G. Galzerano, L. Bonelli, A. Di Lieto, M. Tonelli, and P. Laporta, "Diode-pumped passively mode-locked Yb : YLF laser," Opt. Express **16**, 2922–2927 (2008).
13. F. Pirzio, L. Fregnani, A. Volpi, A. Di Lieto, M. Tonelli, and A. Agnesi, "87 fs pulse generation in a diode-pumped semiconductor saturable absorber mirror mode-locked Yb:YLF laser," Appl. Opt. **55**, 4414–4417 (2016).
14. U. Demirbas, J. Thesinga, H. Cankaya, M. Kellert, F. X. Kärtner, and M. Pergament, "High-power passively mode-locked cryogenic Yb:YLF laser," Opt. Lett. **45**, 2050–2053 (2020).
15. T. Y. Fan, D. J. Ripin, R. L. Aggarwal, J. R. Ochoa, B. Chann, M. Tilleman, and J. Spitzberg, "Cryogenic Yb3+-doped solid-state lasers," Ieee J. Sel. Top. Quantum Electron. **13**, 448–459 (2007).
16. M. Kellert, U. Demirbas, J. Thesinga, S. Reuter, M. Pergament, and F. X. Kärtner, "High power (>500W) cryogenically cooled Yb:YLF cw-oscillator operating at 995 nm and 1019 nm using E//c axis for lasing," Opt. Express **29**, 11674 (2021).
17. K. Yamakawa, M. Aoyama, Y. Akahane, K. Ogawa, K. Tsuji, A. Sugiyama, T. Harimoto, J. Kawanaka, H. Nishioka, and M. Fujita, "Ultra-broadband optical parametric chirped-pulse amplification using an Yb: LiYF_4 chirped-pulse amplification pump laser," Opt. Express **15**, 5018 (2007).
18. S. Melgaard, D. Seletskiy, V. Polyak, Y. Asmerom, and M. Sheik-Bahae, "Identification of parasitic losses in Yb:YLF and prospects for optical refrigeration down to 80K," Opt. Express **22**, 7756–7764 (2014).
19. J. Kim, F. Ludwig, M. Felber, and F. X. Kartner, "Long-term stable microwave signal extraction from mode-locked lasers," Opt. Express **15**, 8951–8959 (2007).
20. M. Endo, T. D. Shoji, and T. R. Schibli, "Ultralow Noise Optical Frequency Combs," IEEE J. Sel. Top. Quantum Electron. **24**, (2018).
21. T. D. Shoji, W. Xie, K. L. Silverman, A. Feldman, T. Harvey, R. P. Mirin, and T. R. Schibli, "Ultra-low-noise monolithic mode-locked solid-state laser," Opt. Vol. 3, Issue 9, pp. 995-998 **3**, 995–998 (2016).
22. U. Demirbas, J. Thesinga, M. Kellert, S. Reuter, M. Pergamnet, and F. X. Kärtner, "40-fs SESAM mode-locked Yb:YLF laser," Opt. Lett. **47**, (2022).
23. W. Bolanos, F. Starecki, A. Braud, J. L. Doualan, R. Moncorge, and P. Camy, "2.8 W end-pumped Yb3+:LiYF4 waveguide laser," Opt. Lett. **38**, 5377–5380 (2013).
24. K. Beil, S. T. Fredrich-Thornton, C. Kränkel, K. Petermann, D. Parisi, M. Tonelli, and G. Huber, "New thin disk laser materials: Yb:ScYLO and Yb:YLF," Conf. Lasers Electro-Optics Eur. (2011).
25. S. T. Fredrich-Thornton, K. Beil, C. Kränkel, K. Petermann, G. Huber, D. Parisi, and M. Tonelli, "Yb:YLF as Active Medium in the Thin Disk Laser," CLEO2011 - Laser Appl. to Photonic Appl. (2011), Pap. CWP7 CWP7 (2011).
26. D. Alderighi, A. Pirri, G. Toci, and M. Vannini, "Tunability enhancement of Yb:YLF based laser," Opt. Express **18**, 2236–2241 (2010).
27. L. E. Zapata, D. J. Ripin, and T. Y. Fan, "Power scaling of cryogenic Yb:LiYF4 lasers," Opt. Lett. **35**, 1854–1856 (2010).
28. D. Rand, D. Miller, D. J. Ripin, and T. Y. Fan, "Cryogenic Yb3+-doped materials for pulsed solid-state laser applications [Invited]," Opt. Mater. Express **1**, 434–450 (2011).
29. D. E. Miller, J. R. Ochoa, and T. Y. Fan, "Cryogenically cooled, 149 W, Q-switched, Yb:LiYF4 laser," Opt. Lett. **38**, 4260–4261 (2013).
30. N. Ter-Gabrielan, V. Fromzel, T. Sanamyan, and M. Dubinskii, "Highly-efficient Q-switched Yb: YLF laser at 995 nm with a second harmonic conversion," Opt. Mater. Express **7**, 2396–2403 (2017).
31. U. Demirbas, H. Cankaya, J. Thesinga, F. X. Kärtner, and M. Pergament, "Efficient, diode-pumped, high-power (>300W) cryogenic Yb:YLF laser with broad-tunability (995-1020.5 nm): Investigation of E//a-axis for lasing," Opt. Express **27**, (2019).
32. R. Peters, C. Kränkel, K. Petermann, and G. Huber, "Broadly

tunable high-power Yb:Lu2O3 thin disk laser with 80% slope efficiency," Opt. Express, Vol. 15, Issue 11, pp. 7075-7082 **15**, 7075–7082 (2007).
33. B. Zhang, B. Zhang, C. Liu, F. Gao, J. He, Q. Wang, S. Kumar, X. Su, Y. Wang, Y. Xie, J. He, and J. He, "17.8 fs broadband Kerr-lens mode-locked Yb:CALGO oscillator," Opt. Lett. Vol. 46, Issue 8, pp. 1892-1895 **46**, 1892–1895 (2021).
34. D. Li, U. Demirbas, A. Benedick, A. Sennaroglu, J. G. Fujimoto, and F. X. Kärtner, "Attosecond timing jitter pulse trains from semiconductor saturable absorber mode-locked Cr:LiSAF lasers," Opt. Express **20**, (2012).
35. U. Demirbas, "Off-surface optic axis birefringent filters for smooth tuning of broadband lasers," Appl. Opt. Vol. 56, Issue 28, pp. 7815-7825 **56**, 7815–7825 (2017).
36. A. Sennaroglu, "Classification of power-degrading mechanisms in an optically pumped four-level laser: an analytical approach," J. Opt. Soc. Am. B-Optical Phys. **36**, 2202–2209 (2019).
37. U. Demirbas, J. Thesinga, M. Kellert, F. X. Kärtner, and M. Pergament, "Detailed investigation of absorption, emission and gain in Yb:YLF in the 78–300 K range," Opt. Mater. Express **11**, (2021).
38. U. Demirbas, J. Thesinga, M. Kellert, M. Pergament, and F. X. Kärtner, "Temperature and doping dependence of fluorescence lifetime in Yb:YLF (role of impurities)," Opt. Mater. (Amst). **112**, 110792 (2021).
39. J. A. Caird, S. A. Payne, P. R. Staver, A. J. Ramponi, L. L. Chase, and W. F. Krupke, "Quantum electronic properties of the Na3Ga2Li3F12:Cr3+ laser," IJQE **24**, 1077–1099 (1988).
40. R. Scheps, J. F. Myers, T. R. Glesne, and H. B. Serreze, "Monochromatic End-Pumped Operation of an Alexandrite Laser," Opt. Commun. **97**, 363–366 (1993).
41. P. W. Roth, A. J. Maclean, D. Burns, and A. J. Kemp, "Directly diode-laser-pumped Ti:sapphire laser," Opt. Lett. **34**, 3334–3336 (2009).
42. J. F. Pinto, L. Esterowitz, G. H. Rosenblatt, M. Kokta, and D. Peressini, "Improved Ti:Sapphire Laser Performance with New High Figure of Merit Crystals," IEEE J. Quantum Electron. **30**, 2612–2616 (1994).
43. U. Demirbas, "Cr:Colquiriite Lasers: Current status and challenges for further progress," Prog. Quantum Electron. **68**, (2019).
44. M. Pollnau, P. Hardman, M. Kern, W. Clarkson, and D. Hanna, "Upconversion-induced heat generation and thermal lensing in Nd:YLF and Nd:YAG," Phys. Rev. B **58**, 16076 (1998).
45. S. Merazzi, R. Gruber, and H. P. Weber, "Thermal Beam Distortions In End-Pumped Nd: YAG, Nd:GSGG, and Nd:YLF Rods," IEEE J. Quantum Electron. **30**, 1605–1615 (1994).
46. J. E. Murray, "Pulsed Gain and Thermal Lensing of Nd:LiYF4," IEEE J. Quantum Electron. **19**, 488–491 (1983).
47. Z. Zhang, Q. Liu, M. Nie, E. Ji, and M. Gong, "Experimental and theoretical study of the weak and asymmetrical thermal lens effect of Nd:YLF crystal for σ and π polarizations," Appl. Phys. B Lasers Opt. **120**, 689–696 (2015).
48. P. J. Hardman, W. A. Clarkson, G. J. Friel, M. Pollnau, and D. C. Hanna, "Energy-transfer upconversion and thermal lensing in high-power end-pumped Nd: YLF laser crystals," IEEE J. Quantum Electron. **35**, 647–655 (1999).
49. H. Vanherzeele, "Thermal lensing measurement and compensation in a continuous-wave mode-locked Nd:YLF laser," Opt. Lett. Vol. 13, Issue 5, pp. 369-371 **13**, 369–371 (1988).
50. V. V Zelenogorskii and E. A. Khazanov, "Influence of the photoelastic effect on the thermal lensin a YLF crystal," Quantum Electron. (Woodbury, N.Y.) **40**, 40–44 (2010).
51. C.-W. Chen, C.-Y. Cho, H.-C. Liang, Y.-H. Fang, H.-C. Liang, and H.-C. Liang, "Investigation of anisotropic thermal lens effect in a dual-polarized Nd:YLF laser," Opt. Lett. Vol. 46, Issue 1, pp. 94-97 **46**, 94–97 (2021).
52. T. J. Carrig, J. W. Hobbs, C. J. Urbina, A. K. Hankla, G. J. Wagner, C. P. Hale, S. W. Henderson, R. A. Swirbalus, and C. A. Denman, "Single-frequency, diode-pumped Yb:YAG and Yb:YLF lasers," Adv. Solid State Lasers (2000), Pap. WC12 WC12 (2000).
53. N. Coluccelli, G. Galzerano, L. Bonelli, A. Toncelli, A. Di Lieto, M. Tonelli, and P. Laporta, "Room-temperature diode-pumped Yb3+-doped LiYF4 and KYF4 lasers," Appl. Phys. B-Lasers Opt. **92**, 519–523 (2008).
54. J. Šulc, H. Jelínková, M. E. Doroshenko, T. T. Basiev, V. A. Konyushkin, and P. P. Fedorov, "Tunability of lasers based on Yb3+-doped fluorides SrF2, SrF2-CaF2, SrF2-BaF2, and YLF," Opt. InfoBase Conf. Pap. (2009).
55. A. Pirri, D. Alderighi, G. Toci, M. Vannini, M. Nikl, and H. Sato, "Direct Comparison of Yb3+:CaF2 and heavily doped Yb3+:YLF as laser media at room temperature," Opt. Express **17**, 18312–18319 (2009).
56. A. Pirri, G. Toci, D. Alderighi, and M. Vannini, "Yb-doped YLF and CaF2 crystal laser at room temperature," Opt. Mater. (Amst). **33**, 200–204 (2010).
57. K. Beil, B. Deppe, and C. Kränkel, "Yb:CaGdAlO4 thin-disk laser with 70% slope efficiency and 90 nm wavelength tuning range," Opt. Lett. Vol. 38, Issue 11, pp. 1966-1968 **38**, 1966–1968 (2013).
58. C. Ma, J. Zhu, K. Liu, Z. Wen, R. Ma, J. Long, X. Yuan, and Y. Cao, "CW and tunable performances of Yb3+:LuAG transparent ceramics with different doping concentrations," Opt. Mater. (Amst). **69**, 190–195 (2017).
59. A. Brenier, A. Eganyan, A. Ródenas, A. G. Petrosyan, D. Jaque, G. Boulon, H. Canibano, and Y. Guyot, "Growth, spectroscopic, and laser properties of Yb^{3+}-doped $Lu_3Al_5O_{12}$ garnet crystal," JOSA B, Vol. 23, Issue 4, pp. 676-683 **23**, 676–683 (2006).
60. S. Nakamura, H. Yoshioka, T. Ogawa, and S. Wada, "Broadly Tunable Yb3+-Doped Y3Al5O12 Ceramic Laser at Room Temperature," Jpn. J. Appl. Phys. **48**, (2009).
61. B. Viana, D. Vivien, F. Balembois, F. Druon, G. P. Aka, P. Georges, P. H. Haumesser, R. Gaumé, and S. Chénais, "Spectroscopy and efficient laser action from diode pumping of a new broadly tunable crystal: Yb^{3+}:$Sr_3Y(BO_3)_3$," JOSA B, Vol. 19, Issue 5, pp. 1083-1091 **19**, 1083–1091 (2002).
62. A. Lucca, F. Balembois, F. Druon, J. L. Doualan, M. Jacquemet, P. Camy, P. Georges, and R. Moncorgé, "High-power tunable diode-pumped Yb^{3+}:CaF_2 laser," Opt. Lett. Vol. 29, Issue 16, pp. 1879-1881 **29**, 1879–1881 (2004).
63. M. Siebold, J. Hein, M. C. Kaluza, and R. Uecker, "High-peak-power tunable laser operation of Yb:SrF2," Opt. Lett. Vol. 32, Issue 13, pp. 1818-1820 **32**, 1818–1820 (2007).
64. B. Viana, F. Balembois, F. Druon, P. Georges, R. Gaumé, and S. Chénais, "Diode-pumped continuous-wave and femtosecond laser operations of a heterocomposite crystal Yb^{3+}:$SrY_4(SiO_4)_3O$?$Y_2Al_5O_{12}$," Opt. Lett. Vol. 30, Issue 8, pp. 857-859 **30**, 857–859 (2005).